

5.1 Radiation Source Performance

5.1.1 Undulator A Performance

Twenty-two insertion devices are now installed in the storage ring (Table 5.1). During 1998, we acquired considerable operating experience with these devices. The first measurements made on undulator A at the APS were reported previously (Cai et al., 1996; Ilinski et al., 1996). This year, additional diagnostics and analyses were performed on the sector 8 undulator (UA2).

The UA2 undulator is a standard 3.3-cm-period APS undulator A (Dejus et al., 1994), which was positioned downstream from the center of the straight section at sector 8. The diagnostics included the angular-spectral measurements of the undulator radiation to determine the undulator radiation absolute spectral flux and the particle beam divergence. The undulator diagnostics setup included a pinhole slit assembly to reduce the incident power and to define the angular acceptance and a crystal spectrometer for absolute spectral flux measurements (Ilinski et al., 1996). All components were mounted on a standard APS optical table with five

Table 5.1. Insertion devices installed at the APS as of August 1998.

Type	Number
3.3-cm-period undulator (undulator A)	17
5.5-cm-period undulator	1
2.7-cm-period undulator	1
1.8-cm-period undulator	1
8.5-cm-period wiggler	1
elliptical multipole wiggler	1

degrees of freedom, so that the setup axis could be adjusted to the axis of the undulator radiation and transverse scans could be performed. The setup was installed in the first optical enclosure (FOE) after two 250 μm Be windows.

The results of the undulator UA2 diagnostics showed that the undulator spectrum measured at different gaps (18.0, 18.5, 19.0 mm) is close to what one could expect. At a gap of 18.5 mm, the measured undulator flux is in a good agreement with the calculated flux (as shown in Fig. 5.1). Flux calculations were performed using the measured undulator UA2 magnetic field profile at a gap of 18.5 mm and the values of the particle beam divergence, particle energy spread, and distance to the source. Comparisons were done for the standard storage ring lattice and for the lattice with low vertical beta function.

For the standard lattice that was used in 1997 ($x = 14.2$ m, $y = 10.0$ m, coupling = 2-4%), the measured absolute flux for the first and third harmonics at a gap of 18.5 mm was within 1% of the calculated undulator flux. The measured flux of the fifth harmonic was 15% less than calculated. For the low-beta lattice that has been used since February 1998 ($x = 16.6$ m, $y = 3.0$ m, coupling = 1.2-1.7%), on-axis flux density of the first harmonic decreased to 92% of that for the standard lattice configuration. The flux density did not change significantly because the horizontal divergence dominates the vertical when two-dimensional convolution is performed. Nevertheless, the larger vertical divergence for the low-beta lattice configuration could require increasing the size of the vertical aperture of the apparatus to obtain the same total photon flux as for the standard lattice configuration.

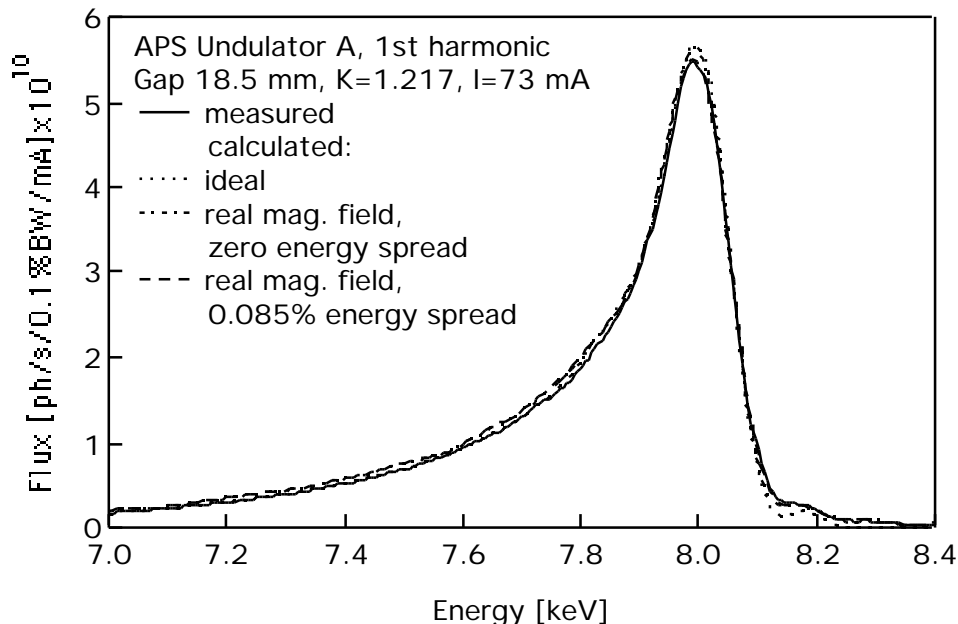


Fig. 5.1 Undulator first harmonic absolute flux at a gap of 18.5 mm. Measured (solid), calculated through the $150 \times 75 \mu\text{m}$ aperture at 28.0 m for $h = 300 \mu\text{m}$, $h' = 24.0 \mu\text{rad}$, for $v = 50 \mu\text{m}$, $v' = 3.9 \mu\text{rad}$: ideal (dotted line), measured magnetic field and zero energy spread (dashed-dot line), measured magnetic field and 0.085% energy spread (dashed line).

Beam divergence was determined from the measured undulator transverse profiles at the detuned harmonic energy, which is less than the fundamental harmonic energy. Measuring angular distribution at the detuned harmonic energy allows one to improve the accuracy of the beam divergence evaluation, because the beam divergence dominates over the intrinsic divergence of the undulator radiation. However, the observed asymmetry of the undulator transverse profiles at the detuned energy may complicate the analysis. From comparison of the profile asymmetries for different storage ring lattice configurations, the assumption was made that the asymmetry effect is due to the nature of the particle beam as opposed to being a property of the undulator.

We found that the undulator second harmonic profile is more sensitive to the horizontal beam divergence changes, and the odd harmonic profiles to the vertical beam divergence. The rms particle beam divergences of $24.0 \pm 0.9 \mu\text{rad}$ (horizontal) and $3.9 \pm 0.3 \mu\text{rad}$ (vertical) were determined for the standard storage ring lattice configuration, and $22.5 \pm 0.9 \mu\text{rad}$ (horizontal) and $5.9 \pm 0.3 \mu\text{rad}$ (vertical) for the low-beta configuration. When beam divergence is determined from the transverse profiles, the main source of the systematic error is the inaccuracy of the beam size.

A particle energy spread of 0.085% was determined from fitting the calculated width of the third harmonic to the measured one. For a 0.085% particle energy spread, the

harmonic widths of the calculated first and fifth harmonics do not exactly match the measured widths of the undulator harmonics. The calculated full width half maximum (FWHM) of the fifth harmonic is 330 eV compared to 366 eV for the measured value.

The diagnostics of undulator A at sector 8 demonstrated once more that the performance of the standard APS ID is quite close to that of an ideal undulator. Also, readily available ID diagnostics equipment with capabilities to measure spectral and spatial radiation distributions proved to be an essential tool at this user facility.

5.1.2 Elliptical Multipole Wiggler Performance

Over the past decade, synchrotron radiation has increasingly been used to probe the magnetic properties of materials. These measurements have generally involved the modulation (or analysis) of the polarization of the incident (or scattered/absorbed) x-ray beams. Techniques, such as circular magnetic x-ray dichroism, core level photoemission, and magnetic Compton scattering, which utilize circularly polarized photons, have attracted particular interest. Because circularly polarized photons couple differently with the magnetic moment of an atom than do neutrons, they are able to provide unique magnetic information not generally accessible by neutron techniques. The development of circularly polarized x-ray diffraction and spectroscopy techniques, however, has been hampered by the lack of efficient sources. Measurements thus far have been primarily taken utilizing off-axis synchrotron radiation from a bending magnet source, which greatly limits incident x-ray flux. The available flux is

particularly important for these types of experiments, due to the inherently small nature of the magnetic x-ray cross section. To increase the available circularly polarized x-ray flux, an elliptical wiggler was first proposed and built by Yamamoto et al. (1989). This device consisted of a series of dipole magnets supplemented by a horizontal magnetic field for tilting particle trajectories up and down to obtain circularly polarized radiation along the axis of the wiggler.

Efficient sources of circularly polarized x-rays should provide both the highest possible flux and degree of circular polarization (P_c). Recently, an elliptical multipole wiggler (EMW) has been designed, built, and operated on the 11-ID beamline of the APS to provide just such characteristics. A comparison of the EMW with other techniques used for the production of circularly polarized x-rays has been given (Lang et al., 1996). The EMW provides a helicity-switchable (<10 Hz), highly polarized, high flux source of hard x-rays ($5 < E < 200$ keV). The first measurements characterizing the performance of this device between 10 and 100 keV have been performed. A detailed description of the EMW facility at the APS has been previously reported (Montano et al., 1995), and only a brief description will be given here. The EMW is based on a design by Gluskin et al. (1995); it has 16 periods and a period length of 16 cm. The 24-mm wiggler gap yields a horizontal deflection parameter (K_y) of 14.6, corresponding to a critical energy of 32 keV and a total wiggler power of 5.4 kW at 100 mA. An electromagnet controls the vertical deflection parameter (K_x), which can be continuously varied from 0.0 to 1.3. The use of the electromagnet allows for rapid helicity reversal up to 10 Hz. The

performance of the EMW was verified by measuring the absolute value of the spectral flux, as well as the degree of linear and circular polarization. The absolute flux and degree of linear polarization measurements were performed by using scattering from a gas in combination with an energy-dispersive detector (Fig. 5.2). This method has been used previously to characterize the spectral flux of undulators (Ilinski et al., 1995; Hahn et al., 1997; and Cai et al., 1996). A direct confirmation that the spectral flux was circularly polarized was made by performing magnetic Compton scattering measurements on an iron sample (Fig. 5.2).

In Fig. 5.3, the measured on-axis flux from this device for two values of K_x is plotted as a function of photon energy and compared

with calculations. The comparison is very satisfactory. The degree of circular polarization (P_C) is obtained for different values of K_x using two independent methods. In the first, the horizontal (I_H) and vertical (I_V) radiation components were measured using the gas-scattering technique for values of $K_x = 0.8, 1.0, \text{ and } 1.3$, $K_y = 14.4$, and over the energy range from 10 keV to 100 keV. From these measurements, the degree of linear polarization is derived using $P_L = (I_H - I_V) / (I_H + I_V)$. Assuming that there is no unpolarized radiation contributing to these measurements, $P_C = [1 - P_L^2]^{1/2}$. In Fig. 5.4, the value of P_C obtained this way is compared with the calculations for an ideal particle trajectory through this magnetic device. The differences are well outside the rms error of the measurement ($< 5\%$) and can only be ascribed to the assumption that

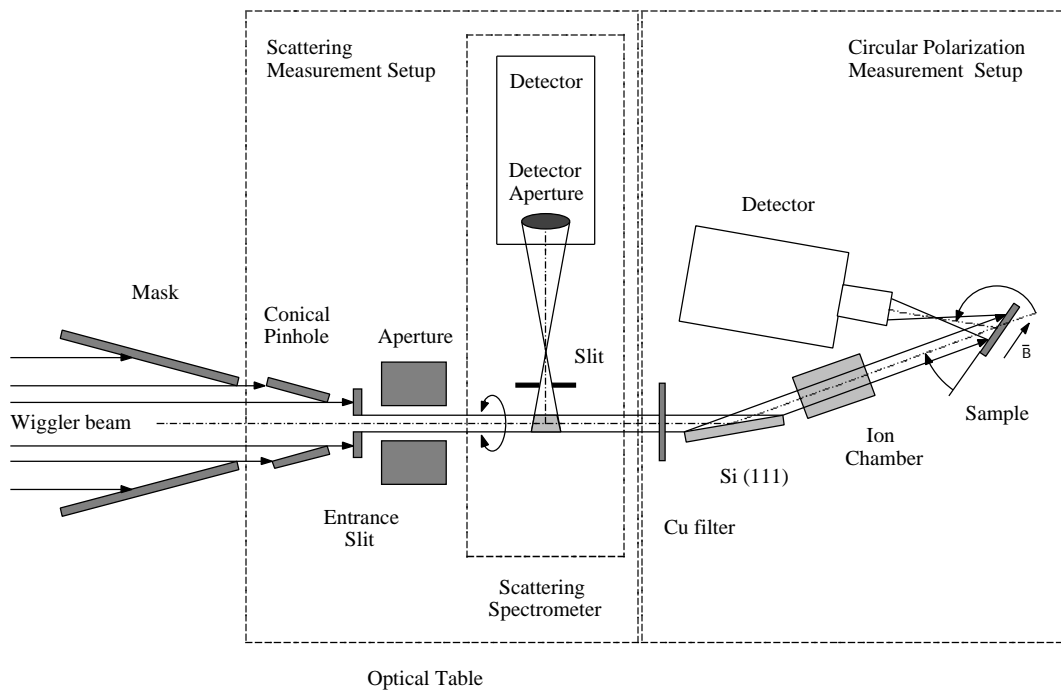


Fig. 5.2 Side view of the experimental setup used for the characterization of circularly polarized radiation from an EMW.

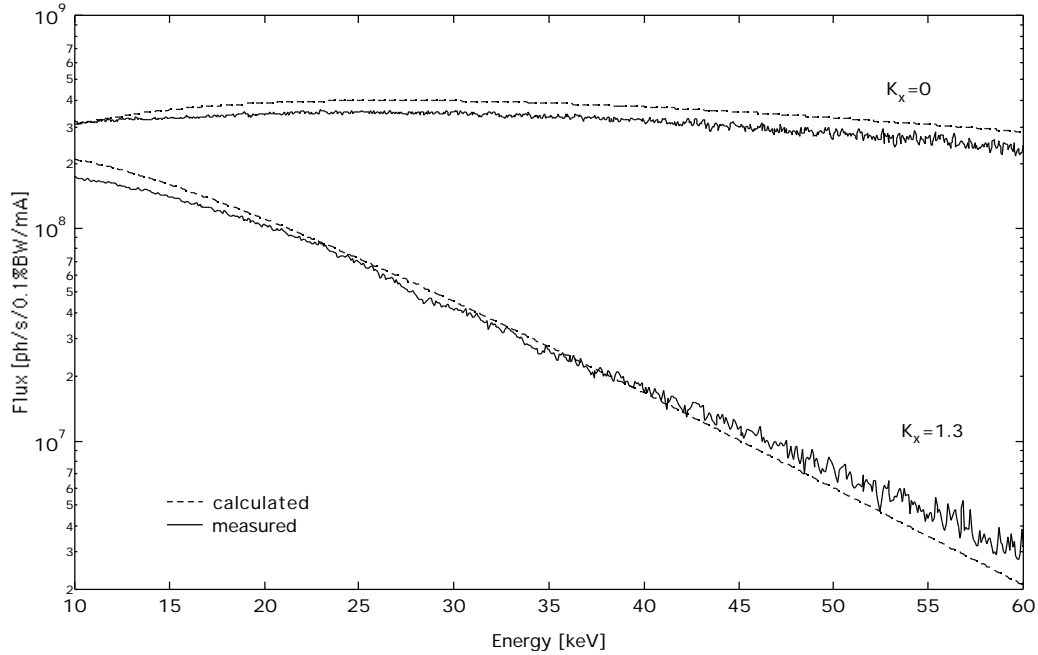


Fig. 5.3 Calculated (dashed) and measured (solid) absolute flux vs. photon energy for $K_x = 0$ and $K_x = 1.3$ through the $75 (v) \times 150 (h) \mu\text{m}$ aperture at 28.75 m. The value of $K_y = 14.4$ for the EMW.

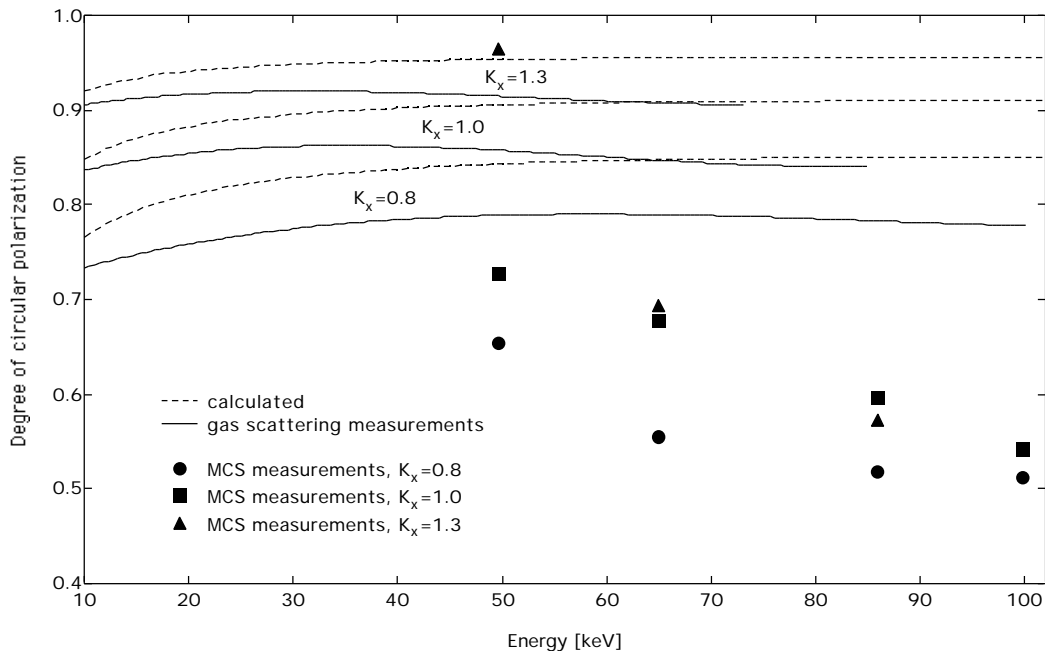


Fig. 5.4 Degree of circular polarization (P_C) vs. photon energy for K_x values of 0.8, 1.0, and 1.3. The value of $K_y = 14.4$ for the EMW.

there was no contribution from unpolarized radiation. A second method was devised in which the P_C is directly measured using magnetic Compton scattering (MCS). The measurements are shown in Fig. 5.4. These measurements do not agree with the results from the gas-scattering measurements or the calculations, except at the lowest energy of measurement. The principal reason behind this discrepancy is attributed to the differing beamline component geometries used in the two methods. In the flux intensive method involving MCS, the beamline apertures were larger, diluting the circularly polarized radiation with linearly polarized radiation. In addition, the apertures used were more transparent at higher energies, increasing the contribution from the linearly polarized photons and thus decreasing the value of P_C at higher photon energies. A detailed discussion on this and other systematic errors in this measurement are given by Ilinski et al. (1997).

While this device is extremely useful, especially at high x-ray energy, in magnetic studies great caution must be exercised in choosing only the central cone of radiation to maximize the degree of polarization. The device is now used regularly by BESSRC CAT users in sector 11.

5.1.3 Circularly Polarized Undulator (CPU)

Both linearly and circularly polarized x-rays have been very successfully applied to the study of magnetic properties of materials. However the applications have been limited primarily due to the lack of energy-tunable,

high-brilliance x-ray beams with adjustable polarization properties. Optics (e.g., quarter wave plates) can be fabricated to simultaneously provide a high-quality beam with adjustable polarization in the energy range above 5 keV starting with a linearly polarized beam from a standard undulator A source. Such optical schemes are harder to implement below 5 keV. To cover this low-energy regime, we are developing, in collaboration with the Budker Institute (Novosibirsk, Russia), a helical undulator that can generate beams of variable (linear or circular) polarization. This undulator is a new type of fully electromagnetic device with the ability to choose either horizontal or vertical plane-polarized or elliptically polarized radiation. The device with a 12.8-cm period is based on a new design that uses both horizontal and vertical electromagnetic poles. The poles are constructed in a C geometry, which allows the insertion device to be installed with a standard APS vacuum chamber (Fig. 5.5). The first harmonic of this device will cover the energy range from 0.4 keV to 3.5 keV. (See Table 5.2 for a list of parameters.) An important and unique feature of a fully electromagnetic device is that it will allow us to generate 100% horizontally ($K_x=0$) or vertically ($K_y=0$) plane-polarized radiation, which will enable many experiments to be performed that otherwise would not be technically feasible. With symmetric deflection parameters ($K_x=K_y$), the on-axis radiation will be ~100% circularly polarized. Figure 5.6 shows the brilliance range of the CPU in linear polarization mode, together with that of a 5.0-cm-period elliptical device planned for the Advanced Light Source (ALS EPU). The details on the location and

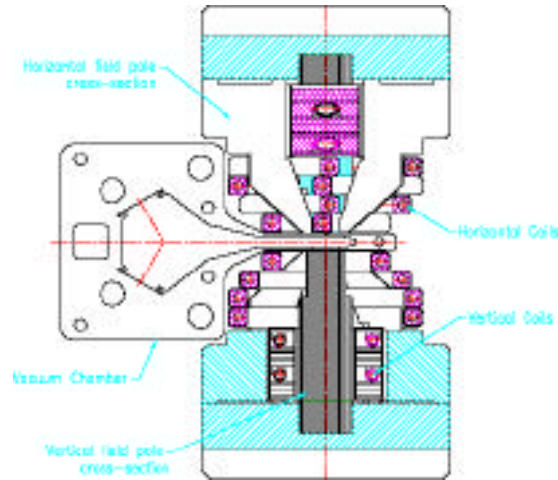


Fig. 5.5 Cross section of the CPU poles nesting around the ID vacuum chamber showing the horizontal and vertical coils.

Table 5.2. Parameters of the 12.8-cm-period intermediate energy CPU.

Circularly Polarized Undulator	
Period	12.8 cm
Number of full vertical poles	35
Number of full horizontal poles	36
Overall length	2.4 m
Vertical pole gap	11 mm
Maximum magnetic field	0.24 Tesla
Energy range	0.5-3.0 keV
Switching frequency	0 – 10 Hz
Switching rise time (including overshoot)	< 20 ms
Electromagnet dc stability	< 1%
Maximum total power	800 W
Maximum power density	17 W/mm ²

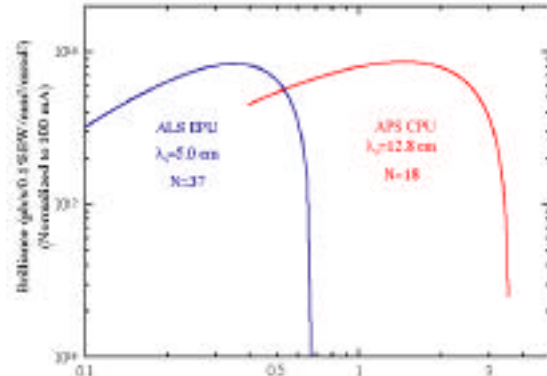


Fig. 5.6 Comparison of helical undulator brilliance.

installation of the CPU are discussed in the next section.

5.1.4 Simultaneous Operation of Two Undulators

At the APS, the straight sections in the storage ring have a length of 5.0 m, thus permitting the installation of two undulators of maximum length 2.4 m. Such configurations of two undulators can enhance the capabilities of the APS. Two unique configurations have been planned. In the first, two 2.4-m-long undulators A will be installed on the straight section in sector 1. The beam, with nearly double the power (and power density), will permit the evaluation of the ultimate performance of nitrogen-cooled Si optics and water-cooled diamond optics. This R&D will support user operations at stored beam currents much higher than 100 mA.

In the second configuration, two undulators with dissimilar periods will be installed on the same straight section to derive two independent radiation beams with different spectral properties. The proposed installation on sector 4 will have undulators with periods of 3.3 cm and 12.8 cm, providing radiation above and below 5 keV and covering the energy range from 0.5 to 50 keV.

The sector 4 beamline will be the first at the APS designed explicitly to operate with two undulators simultaneously. By inserting a weak horizontal steering magnet between the two tandem IDs, a deflection or 'dogleg' can be produced in the particle beam orbit. This will cause the radiation from the two undulators to be horizontally separated on the experimental hall floor. The hard x-ray

range will be covered using the APS standard undulator A. A custom-built 12.8-cm-period variably polarized undulator (see previous section) will be used for the intermediate energy x-ray range. An 8-mm beam separation in the FOE at approximately 30 meters from the center of the straight section is desired. This will require a dipole electromagnet sufficient to steer the beam through 270 microradians. Three permanent magnet dipoles will be installed: one in front of the undulators, one between the undulators, and one after the undulators to create the dogleg.

5.1.5 5-mm Chamber and Undulator Measurements at 8.5-mm Gap

In January 1998, a 5-meter-long 5-mm-aperture ID vacuum chamber was installed in sector 3 to allow the 2.7-cm-period undulator to achieve smaller gaps. To enable operation of the storage ring without sacrificing lifetime, a low-beta lattice ($x = 16.6$ m, $y = 3.0$ m) tuning was developed by ASD. The 5-mm-aperture vacuum chamber allowed the minimum undulator gap to be decreased to 8.5 mm. This extended the x-ray energy range and filled in gaps in the tuning curve, as shown in Fig. 5.7, where the dotted sections of the lines show the additional capability allowed by the smaller minimum gap. Experimental measurements were made of the photon output at a variety of energies, and the measurements agreed well with calculated predictions.

This device delivers higher brilliance than the 3.3-cm-period undulator A in the energy range above 10 keV. The availability of the 5-mm-aperture vacuum chamber will enhance the capability of the user scientific

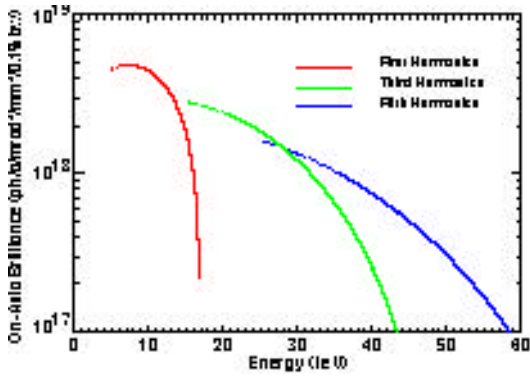


Fig. 5.7 Tuning curves for the 2.7-cm-period undulator. The dotted line extensions of the curves show the increase in tuning range achieved by decreasing the minimum gap to 8.5 mm.

programs at the APS. Many of the CATs have expressed interest in using the small aperture chamber, which will impact two distinct scientific areas: (1) deriving photon energies down to 2.0 keV using the existing 3.3-cm-period undulator A (which is of special interest to the biological and environmental research communities to reach the absorption edges of elements such as sulphur), and (2) deriving high-brilliance photons at higher energies using the 2.7-cm-period undulator in conjunction with the small aperture vacuum chamber. The impact will be primarily in condensed matter and materials science research, which require both high brilliance (or coherence) at higher photon energies (in comparison with the performance of the 3.3-cm-period undulator).

These new capabilities will impose higher power-handling requirements on the first optics in the beamlines, an area of continuing R&D in XFD (see section 5.3).

5.1.6 Storage Ring Installation – Phase-2

Vacuum chambers for IDs have been installed in 21 sectors of the storage ring; 35 sectors are available for ID beamlines. In 1998, efforts began to fabricate most of the components necessary to complete the ID instrumentation for the remainder of the storage ring. Ten additional 5-meter-long 8-mm-aperture vacuum chambers are being fabricated, and eleven undulator A type (3.3 cm period) magnetic structures were procured from STI Optronics for delivery beginning in December of 1998. The CPU (described in section 5.1.3) will be installed in sector 4. Electrical racks and power distribution have been added to the storage ring tunnel roof to accommodate the installation of IDs in the remaining sectors.

New Gap Separation Mechanism

A new design for an ID gap separation mechanism has been completed and procurement of components to assemble a prototype is underway. The goal of the new design is to improve ID gap positioning accuracy while reducing mechanical complexity to reduce cost. The design uses four drive motors, one for each end of each jaw, to move each end of the top and bottom jaws independently—thereby simplifying the mechanical drive trains while allowing fine adjustments to the parallelism of the jaws. The load bearing frame is assembled from stress-relieved welded structural steel beams (Fig. 5.8). The system has been designed to be compatible with the existing undulator A magnetic assemblies and to allow a minimum gap under load of 10 mm.

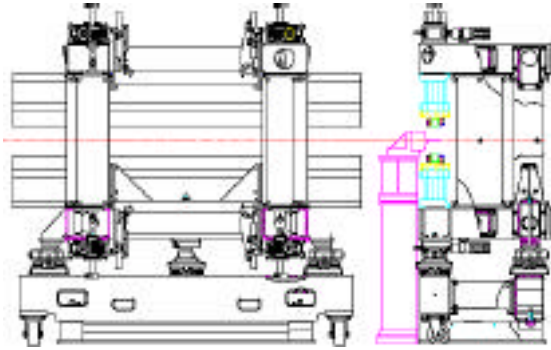


Fig. 5.8 New gap separation mechanism for undulator A.

The frame is extremely rigid; finite element calculations show a deflection of less than 3 μm when the 3.3-cm-period magnetic structure is closed to an 8.5-mm gap.

5.1.7 Collaborations

BESSY Chambers

For several years, the ID group of XFD has collaborated with the staff of the Berliner Elektronenspeicherring-Gesellschaft für Synchrotronstrahlung (BESSY), located in Berlin, Germany, to design and fabricate ID vacuum chambers for the BESSY II project. These chambers used the innovative technology developed by the APS for small aperture vacuum chambers. In 1998 this project was completed; ten chambers were delivered to Berlin for installation into the storage ring. One of these chambers is shown in Fig. 5.9.

DESY Chambers

The Deutsches Elektronen-Synchrotron (DESY), located in Hamburg, Germany, is building a vacuum ultraviolet (VUV) FEL based on the TESLA Test Facility linear accelerator. The APS is an official partner in this project. Towards this objective, XFD is designing and fabricating the small-aperture extruded-aluminum vacuum chambers that will be used for the FEL undulators. Seven 9.5-mm-aperture chambers, each 4.516 m long, are being built. Figure 5.10 shows the first chamber after preliminary machining. The project is expected to be completed in the spring of 1999, and the FEL tests will be performed during the fall of 1999. The FEL operated at 1 GeV is expected to produce radiation with a wavelength of 70 nm.



Fig. 5.9 One of the vacuum chambers designed and built for BESSY II.

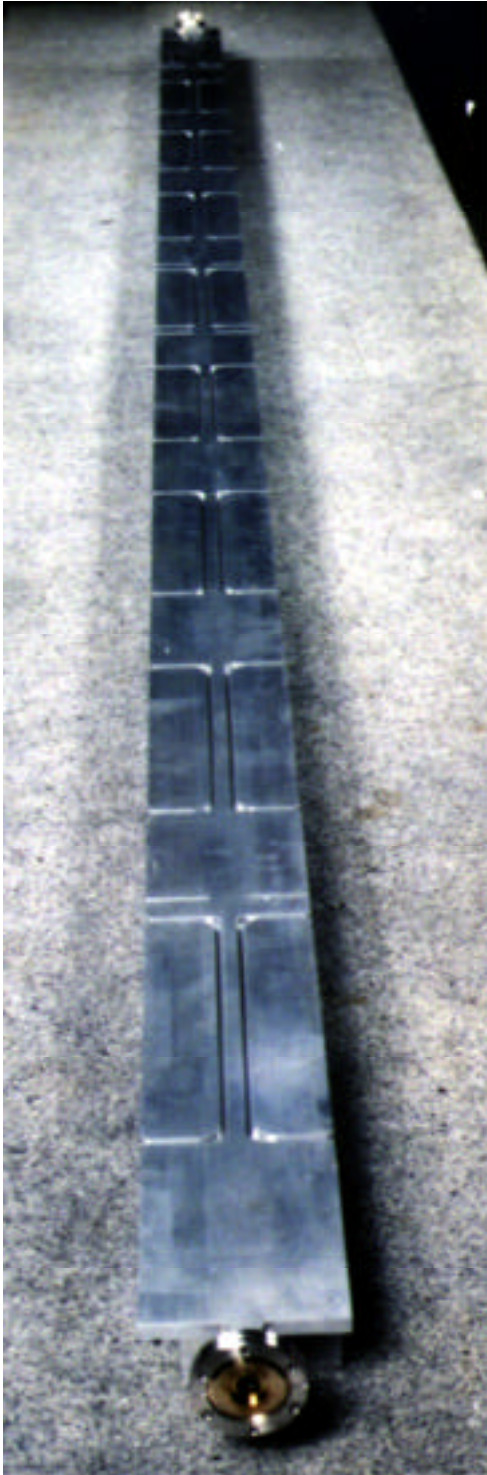


Fig. 5.10 One of the vacuum chambers designed and built for the DESY FEL project.